Conference Paper, Published Version

Murphy, Edna; Walker, James

Shear-driven flushing and circulation in a marina in the United Arab Emirates

Zur Verfügung gestellt in Kooperation mit/Provided in Cooperation with:
TELEMAC-MASCARET Core Group

Shear-driven flushing and circulation in a marina in the United Arab Emirates

Enda MURPHY, James WALKER

Sogreah Gulf – Artelia Group

Dubai, United Arab Emirates

enda.murphy@ae.arteliagroup.com

Abstract— **Flushing or residence times are typically used to assess water quality potential in marinas and other semi-enclosed water bodies. Recent publications have focussed on developing and revisiting general guidelines to improve water exchange in tidal marinas by optimizing basin and entrance geometry. However, these guidelines are based on specific cases where water exchange is strongly tide-driven and frequently do not apply to micro-tidal sites. In this work, we focus on a real-world example of a marina on the edge of a micro-tidal channel, where water exchange is strongly influenced by transverse velocity shear at the interface between the channel and the marina basin. A TELEMAC-2D hydrodynamic model of the channel and marina basin was developed, calibrated and validated using field measurements of current speeds and water levels. The numerical model was used to assess flushing times for different marina and entrance configurations. The results demonstrate a particular example where dead-zone models of water exchange, traditionally applied to evaluate mass transport in rivers and groyne fields, provide a better means to guide optimization of basin and entrance geometry.**

I. INTRODUCTION

Flushing or residence times have historically been used as a first step in assessing water quality in marinas, harbours and coastal basins [2, 5, 9, 20, 22, 28, 29]. Recent publications have offered guidance in relation to optimal basin geometries (e.g. plan form factor, aspect ratio, tidal prism ratio, curvature, relative entrance area) to help achieve rapid renewal [2, 5, 28, 29]. However, these guidelines have been developed for the particular case where water exchange is strongly tide-driven and are not widely applicable, particularly in micro-tidal regions such as the Persian Gulf, where mean spring tidal ranges are typically less than 2m.

For marinas in micro-tidal areas, the tidal prism is seldom sufficient to ensure adequate water renewal by purely tide-driven exchange. Where water exchange is dominated by shear-driven circulation and lateral transfer of momentum at the interface between the marina and the adjacent water body (i.e. a mixing layer), there is a strong analogy to groyne fields and other cases involving flows containing quasi-stagnant peripheral areas (dead zones). In these cases, dead-zone models for mass transport may present a better alternative to guide optimization of basin and entrance geometry.

In this paper, a case study is presented whereby a numerical hydrodynamic model was used to evaluate flushing times in a marina on the edge of a micro-tidal channel in the United Arab Emirates. A number of basin and entrance geometries were tested to investigate the impacts on residence times. We investigate the applicability of dead-zone models of water exchange, traditionally used to evaluate mass transport in rivers and groyne fields, to the case of a marina on the edge of a micro-tidal channel.

II. DEAD-ZONE MIXING PROCESSES AND MODEL FOR WATER EXCHANGE

The effect of quasi-stagnant, or "dead" zones on water exchange and mass transport in rivers has been the subject of considerable research over the past 35 years [1, 4, 6, 7, 13, 14, 24, 26, 27, 30, 31, 35]. Dead zones, which are defined by [24] as local areas of the flow cross section with relatively still water, or no net downstream velocity, are created in rivers by the presence of meanders [27], natural or manmade peripheral embayments (including marinas) [32], groyne fields [32, 33, 34], vegetated zones [10, 11, 12, 13, 14, 19, 21], hyporheic zones [13, 21, 35], pools and riffles [13].

Dead zones on the sides of channels result in shear flow at the interface with the main channel and an associated inflection point in the streamwise velocity profile. The latter is a characteristic of mixing layers, commonly observed in terrestrial [25] and aquatic vegetated flows [10], and is a prerequisite criterion for instability [16, p. 499]. Mixing layers are susceptible to Kelvin-Helmholtz instability, such that transport across the layer is typically dominated by large scale vortex structures [10, 32]. The formation of vortices and the efficiency of exchange between the dead zone and the main channel, which are separated by the mixing layer, are subject to local flow conditions and the geometry of the dead zones [12, 30, 32]. The rate of renewal of water in the dead zone is also strongly influenced by secondary gyres [32].

Most dead zone models consider exchange between stagnant zones and the main stream to be well represented by a first order process [4, 7, 30, 32]:

$$\frac{\partial C}{\partial t} = b(C - C_s) \tag{1}$$

where C and C_S are the concentration of a conservative solute in the dead zone and main stream, respectively, t is time, and b is an exchange coefficient with dimensions T^{-1}. For a dead

zone of uniform concentration, the inverse of the exchange coefficient provides a measure of the time scale for water renewal within the dead zone, commonly referred to as the mean residence time, T_R. For an ideal (plane) mixing layer [25], the exchange coefficient is known to be a function of the difference between the net streamwise velocity in the main stream and the dead zone, $\Delta U = U - U_M$ [12, 19], and the width of the layer. Assuming zero net flow in the dead zone and considering that the thickness of the plane mixing layer is constrained by the width of the dead zone perpendicular to the flow, W (Fig. 1), it follows that

$$b = b_{ideal} = \frac{kU}{W} \tag{2}$$

where k is a dimensionless coefficient, referred to as an "entrainment coefficient" by [30, 32]. In the case of transverse mixing between a main stream and a peripheral dead zone of finite depth (*i.e.* a real mixing layer), the formation of large scale vortices (which controls the rate of exchange) is also dependent on the limiting water depth [32]. Using mass conservation principles, Weitbrecht *et al.* [32] showed that in such cases, the exchange coefficient is given by the dead-zone model as

$$b = \frac{kU}{W} \frac{h_E}{h_M} \tag{3}$$

where h_E is the depth at the entrance to the dead zone and h_M is the average depth in the dead zone, as illustrated in Fig. 1. Thus, by determining the coefficient k, shear-driven exchange between the main stream and a side-embayment and the associated mean residence times can be evaluated. For the specific case of a tidal channel, $U = U(t)$. Here, we make the assumption that (3) holds approximately for $U = U_{rms}$, implying quasi-steady state conditions.

Valentine and Wood [30] considered a value of $k = 0.02$ to be generally appropriate for a rectangular cavity in a channel bed, consistent with previous experiments for side cavities (cited in [30]). For a range of groyne field geometries and configurations, Weitbrecht *et al.* [32] determined via experiments entrainment coefficients ranging from 0.012 to 0.051. They developed an empirical relationship between k and the dead zone geometry, through a nondimensional shape parameter that is fundamentally analogous to a hydraulic radius:

$$R_D = \frac{WL}{h_S(W + L)} \tag{4}$$

where L is the length of the dead zone and h_S is the flow depth in the main stream (Fig. 1). Weitbrecht *et al.* [32] contend that the formation of large scale vortices (which controls the rate of exchange) is dependent on the stability of the mixing layer governed by the ratio of the width (~ L, W) to the water depth in the channel (~ h_S). In the specific case of a shallow marina on the edge of a deeper channel, with one or more breakwaters partially protruding across the entrance (Fig. 1), we argue that the length scales controlling the development of vortices are the entrance width, L_E, the

average depth in the marina, h_M, and W. Thus, we propose a modified shape parameter:

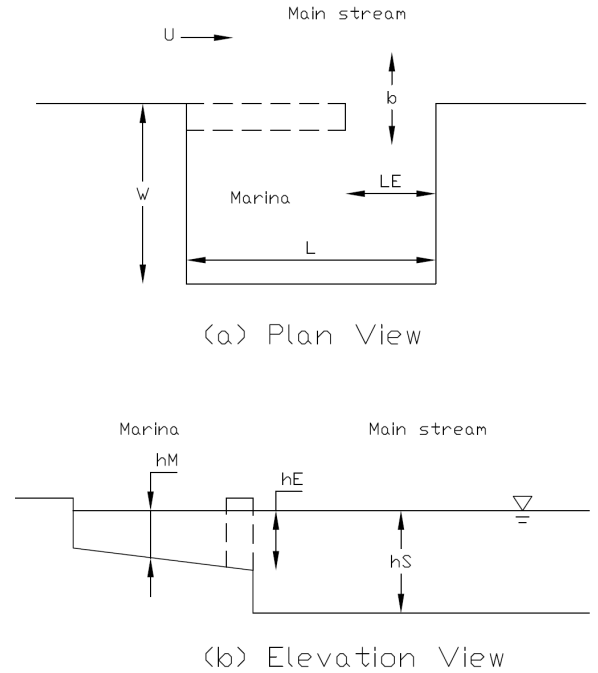$$R_{DM} = \frac{WL_E}{h_M(W + L_E)} \tag{5}$$

Figure 1. Schematic of a marina on the edge of a channel.

In this paper, we use a TELEMAC-2D numerical model to evaluate entrainment coefficients for a marina on the edge of a tidal channel and to investigate the relationship with the marina and entrance geometry.

III. NUMERICAL MODEL INPUTS AND METHODOLOGY

A. Model Setup

The computational domain of the TELEMAC-2D [8, 15] version 5.9 model was set up to reflect available boundary condition data and the location of the marina site. The extent of the model domain is shown in Fig. 2. The triangular computational mesh for the post-development (base case marina layout) scenario, was constructed using the Blue Kenue™ software tool [3]. The mesh consists of more than 20,000 triangular elements, with increased resolution at the project site (characteristic element edge lengths of 5 to 10m).

The coastline and bathymetry of the model were generated from:

- Detailed topographic and bathymetric surveys of the site and adjacent channels;

- Digitized geo-referenced satellite images;

- AutoCAD drawings of the proposed marina layouts for post-development scenarios.
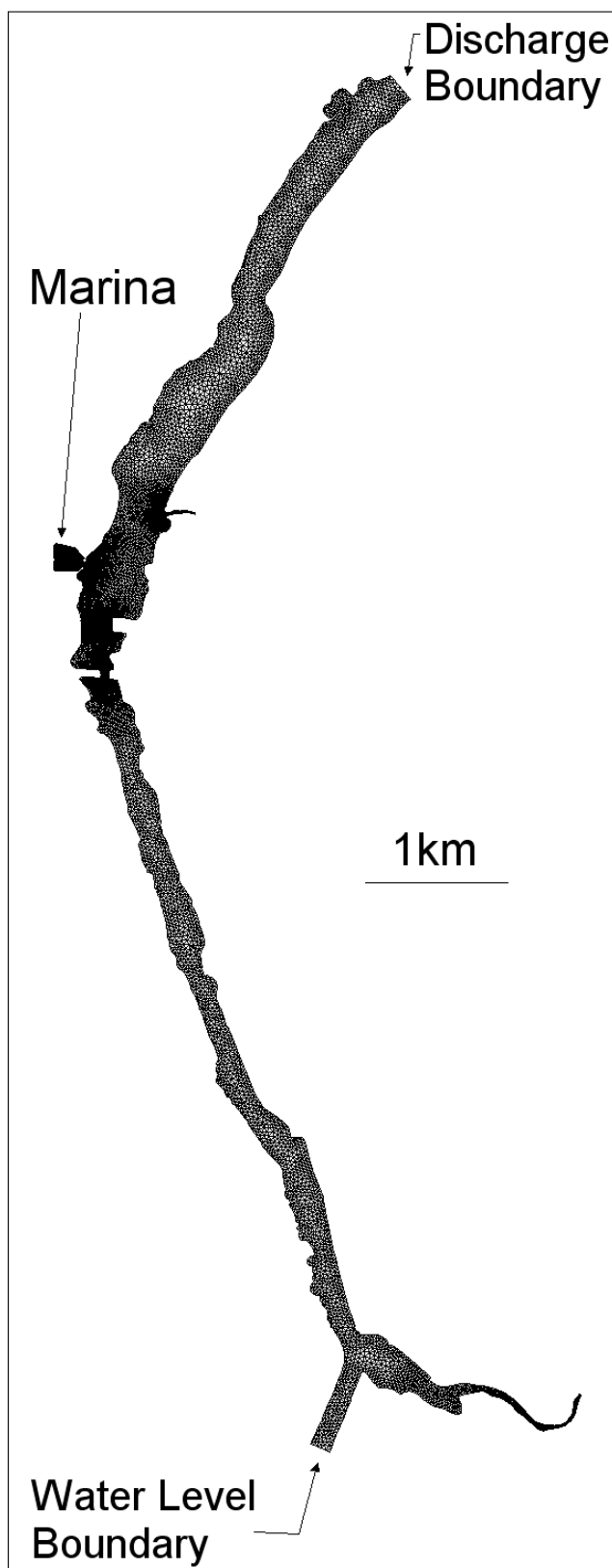
Figure 2. Numerical model domain, mesh and boundary conditions.

The model bathymetry for the pre-development scenario, which was used to calibrate and validate the model, is shown in Fig. 3, referenced vertically to the project datum (approximately equivalent to mean sea level). Open water boundary conditions were applied as follows (as indicated in Fig. 2):

- A temporally varying water level along the southern boundary; and

- Temporally varying water levels and currents (velocity component normal to the boundary) along the northern boundary.

B. Field Data

To support the numerical modelling, a programme of hydrographic field surveys was implemented for the project, which included:

- Measurement of directional current speeds using bed-mounted acoustic Doppler current profilers (ADCPs) at three locations in the channel; and

- Measurement of water levels using calibrated tide gauges at three locations in the channel.

Details of the ADCPs (ADCP01, ADCP02 and ADCP03) and tide gauges (SG01, SG02 and SG03) are listed in Table I. The locations of the field instruments in the tidal channel are shown in Fig. 3.

Ideally, hydrographic field measurements to support calibration and validation of a tidal hydrodynamic model should be carried out for a minimum period of 15 days to capture variations over a full spring-neap tidal cycle. However, due to project time constraints, the recording durations were shortened to approximately 5 days and 11 days for the ADCPs and tide gauges, respectively.

Since field data was available for only a limited duration, harmonic constituents were estimated from the field data and then used to approximate the time series of water levels and currents over an extended period spanning a full spring-neap tidal cycle.

C. Model Calibration and Validation

The model was calibrated using the field measurements of water levels and currents. Model input variables, such as bed roughness coefficients and turbulence parameters, were adjusted incrementally within appropriate ranges and simulations were implemented for the period corresponding to the field surveys. The final calibrated model parameters (Table II) were then selected based on goodness-of-fit and visual inspection of the time series measurements and predictions at the stations closest to the development site (SG02 and ADCP02).

Observed and predicted free surface elevations, depth-averaged current speeds and depth-averaged current directions are shown for the calibration period (19/8/2010 – 24/8/2010 for currents and 17/8/2010 – 28/8/2010 for water levels) in Fig. 4 for the locations nearest the site (SG02 and ADCP02). Visual inspection indicates good agreement between the field measurements and model predictions, with

TABLE I.   FIELD INSTRUMENT DETAILS

| Station ID	Instrument Type	Location	Approx. Depth (m)	Recording Interval (min)
ADCP01	Acoustic Doppler current profiler	North channel entrance	6.4	10
ADCP02	Acoustic Doppler current profiler	Adjacent to site	6.9	10
ADCP03	Acoustic Doppler current profiler	South channel entrance	6.0	10
SG01	Tide gauge	North channel entrance	n/a	10
SG02	Tide gauge	Adjacent to site	n/a	10
SG03	Tide gauge	South channel entrance	n/a	10
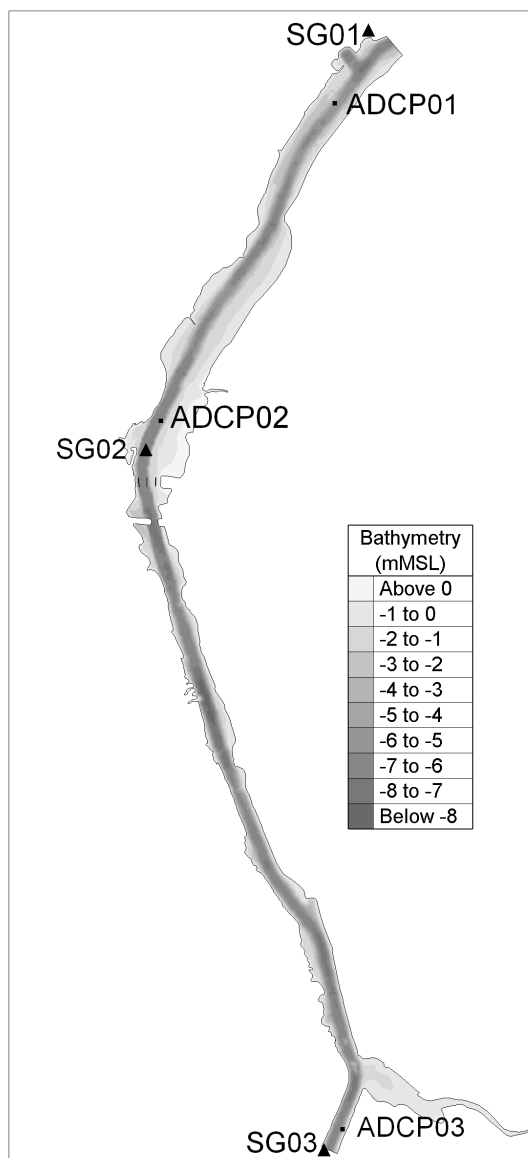
Figure 3. Model bathymetry and locations of field instruments.

the phasing and magnitude of water levels, peak current speeds and directions all captured accurately by the hydrodynamic model. This assessment is supported by the statistics of the fit, with correlation coefficients for measured versus predicted values close to 1 ($R^2 = 0.997$ and 0.848, for water levels and depth average current speeds, respectively). Predicted and observed rms depth average current speeds differ by less than 2.5% (0.43m/s observed versus 0.44m/s predicted).

Once the final model parameters were established through calibration, a full spring-neap tidal period was simulated using the extended time series, and goodness-of-fit between the reconstructed time series and model-predicted values was reassessed (validation). Results showed that the calibrated hydrodynamic model accurately captured the spring-neap variation in water levels and depth-averaged currents. The phasing and magnitude of water levels, peak current speeds and directions were all found to be in good agreement for the validation period, with correlation coefficients $R^2 = 0.996$ and 0.890 for water levels and depth average current speeds, respectively. Differences in rms depth average current speeds were less than 1.5%.

D. Flushing Assessment Methodology

Flushing was assessed by introducing a conservative (i.e. non-decaying in time) tracer to the hydrodynamic model with an arbitrary initial value of 100 everywhere within the marina basin. The hydrodynamic model was then used to simulate the advection and dispersion of the tracer over a 15-day period beginning on a neap cycle, to quantify the exchange with outside waters. The simulation was chosen to begin during neap conditions as this typically provides the most conservative time estimate of tide-driven water exchange.

E. Marina Layouts

To evaluate the flushing efficiency of different marina layouts and configurations, the following four scenarios were investigated using the numerical model (Fig. 5):

- Layout 1 – base case marina layout;

- Layout 2 – raised bed elevations in southern parts of the marina basin;

TABLE II.   SUMMARY OF MODEL PARAMETERS

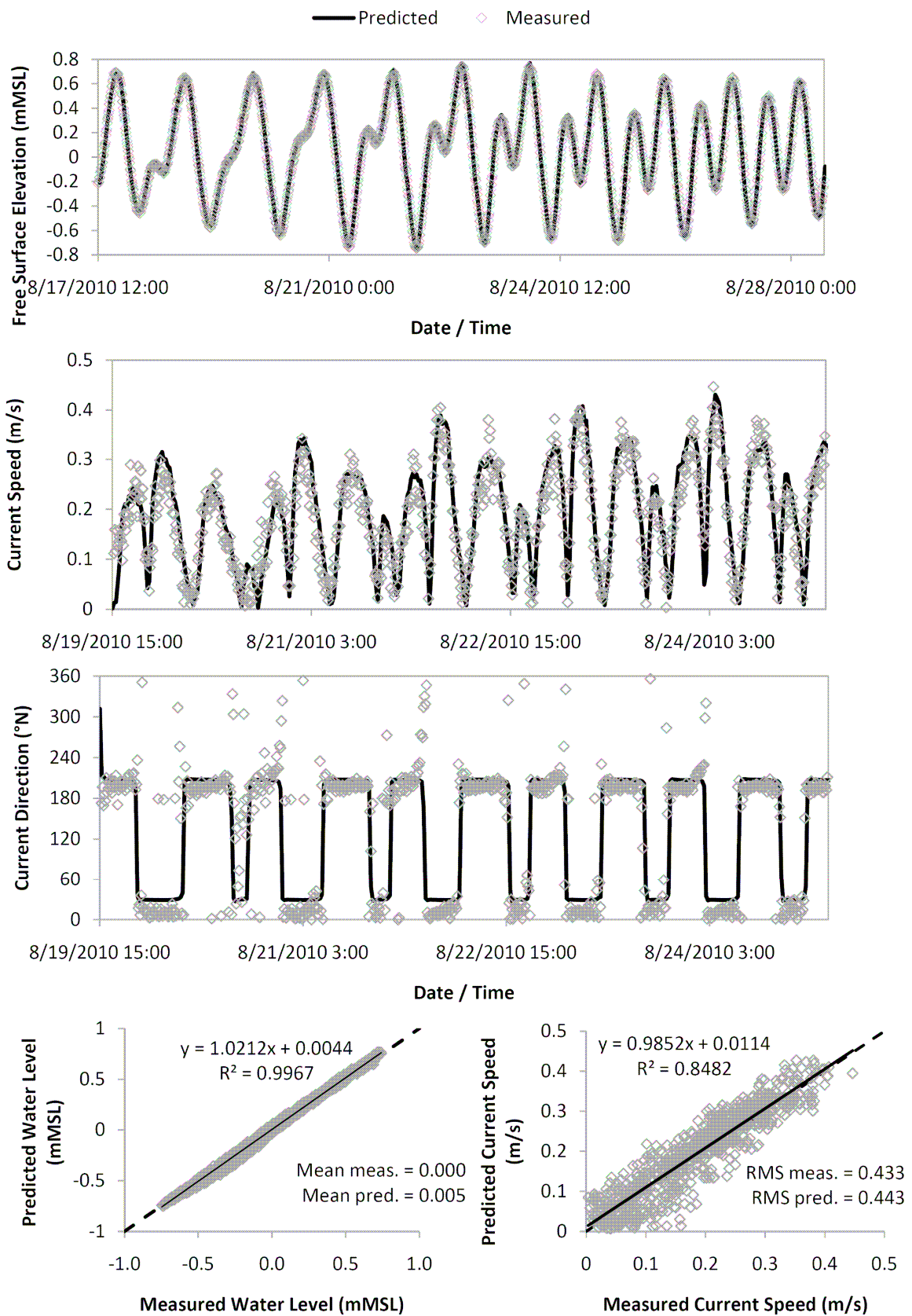| Model Process	Parameter and Units	Range of Values Tested During Calibration	Final Calibrated Value
Bed friction	Chezy coefficient ($m^{1/2}$/s)	25 to 60	60
Turbulence model	Constant eddy viscosity, v_T (m^2/s)	0.01 to 0.1	0.01
Physical properties	Seawater density (kg/m^3)	1030	1030
Wetting / drying	Tidal flats	Wetting / drying included	Wetting / drying included

Figure 4. Time series and regression analysis of field measurements and model predictions for the calibration period.
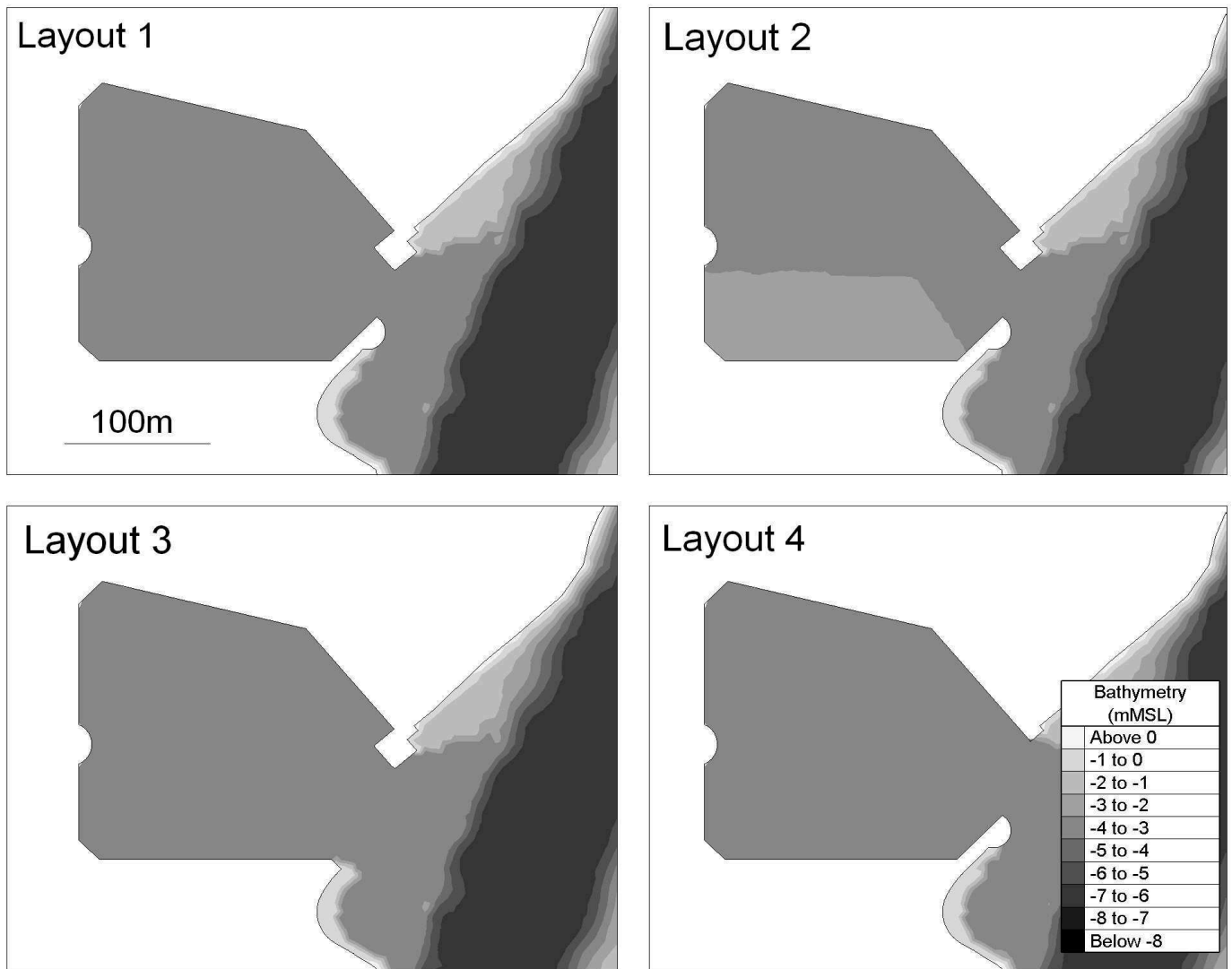
Figure 5. Marina layouts, entrance configurations and bathymetries investigated using the numerical model.

- Layout 3 – no breakwater on the southern side of the marina entrance;
- Layout 4 – no breakwater on the northern side of the marina entrance.

IV. RESULTS AND DISCUSSION

Results for each of the numerical simulations are listed in Table III. Fig. 6 shows the tide- and basin-averaged relative tracer concentration, C/C_0, versus time (normalized by the semi-diurnal tidal period, $T_P \approx$ 12h) for each of the simulations. Tide averaged values were computed by twice applying a running average filter to the results, using a time window $T_{mean} = T_P$. For each layout, the exchange coefficient, b, was evaluated from a least squares exponential fit to the basin- and tide-averaged tracer concentration (*e.g.* as described in [27]).

The formation of large scale vortices at the interface between the marina and the main channel was observed for all layouts, and was most evident in the results for Layout 3 (Fig. 7), which incidentally, was the layout with the widest entrance and the shortest mean residence time. This suggests shear-generated circulation is the dominant exchange mechanism.

Fig. 8 shows the entrainment coefficient, k, determined from (3) and the best fit b for each simulation, plotted against the modified shape parameter in (5). There is reasonable (although not statistically significant [23]) correlation between k and R_{DM} ($R^2 = 0.7221$, $n = 4$, $\alpha = 0.05$), suggesting the dead zone model and the length scales adopted in the modified shape parameter are generally valid. By contrast, there is no apparent correlation between residence times and R_D (Table III) or other traditional indicators for tide-driven exchange (*e.g.* tidal prism ratio, relative entrance area [5]).

TABLE III.   LAYOUT DEFINITIONS AND NUMERICAL MODEL RESULTS

Layout	U_{rms} (m/s)	W (m)	L_E (m)	L (m)	a (m²)	A (m²)	h_E (m)	h_M (m)	h_S (m)	$b \times 10^6$ (s⁻¹)	T_R (days)	k (–)	R_D (–)	R_{DM} (–)
1	0.2	215	35	160	112	34320	3.2	3.2	7.0	2.5	4.8	0.005	13.1	9.4
2	0.2	215	35	160	112	34320	3.2	2.9	7.0	3.4	3.4	0.007	13.1	10.3
3	0.2	215	77	160	246	34430	3.2	3.2	7.0	7.0	1.7	0.015	13.1	17.7
4	0.2	215	56	160	179	34570	3.2	3.2	7.0	2.6	4.3	0.006	13.1	13.9 (7.7) [a]

a. Values in parentheses are adjusted for a central entrance, as suggested (for tide-driven exchange) in [5].

The computed values of k are generally lower than the ranges determined experimentally by [30] and [32]. This may be explained by the fact that, for the layouts investigated, the large scale vortices did not penetrate fully to the inner side of the marina. This inhibits mixing in areas of the marina not encompassed by the mixing layer, resulting in lower values of k. It is also important to note that the experiments by [30, 32] were confined to unidirectional flows. For the numerical simulations presented in this paper, part of the mass of tracer removed from the marina during flood tide was observed to return during ebb flow conditions, increasing the mean residence time and leading to reduced values of k. This suggests that further work is needed to investigate how the quasi-steady approximation, $U = U_{rms}$, affects the dead zone model predictions, since observations have shown that mass transfer rates for oscillatory flows may be significantly different to those for comparable unidirectional currents [17].

The lower values of k are consistent with the value of turbulent diffusivity for the tracer implemented in the numerical model, $D_T = 0.01 \mathrm{m}^2$/s, which gives a turbulent Schmidt number (the ratio of the eddy viscosity to the turbulent diffusivity of the tracer) $Sc_T = 1$. This falsely implies that mass is transported as efficiently as momentum, when typically $Sc_T < 1$ for shear layers [12, and references therein].
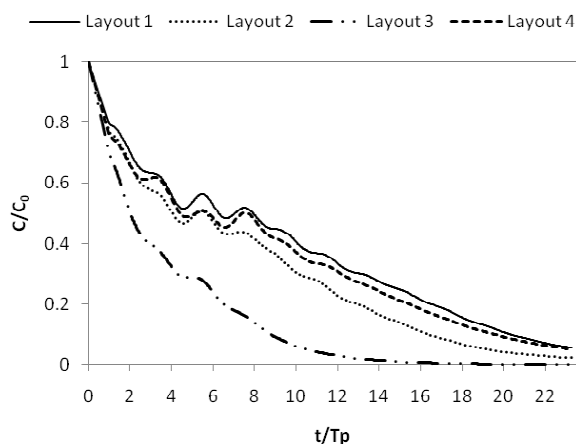

Figure 6. Computed normalized tide- and basin-averaged relative tracer concentrations.

As k is a measure of the efficiency of transport across the mixing layer, it is useful to consider factors affecting the development of the layer, one of which is that its growth may be constrained by the time scale for reversal of flows. However, the length of the marina entrance (L_E) also plays a role in determining k. For groyne fields and dead zones in rivers, the entrainment coefficient in upstream areas is known to differ significantly from values downstream, which are generally quite constant [1, 31, 32]. This is because the mixing layer is not fully developed over short distances [11] and because particles do not have sufficient time to sample the full range of velocities in the main stream and dead zones (i.e. Fickian conditions have not been reached). For marinas with short entrances, fully developed mixing layers may never be practically realised, due to impingement on the downstream edge. In this case, complex feedback mechanisms not represented by the dead zone model may also persist [18].
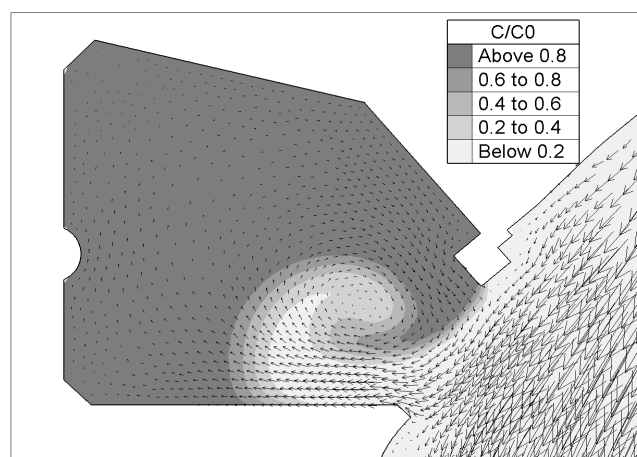

Figure 7. Snapshot of relative tracer concentrations and current vectors for Layout 3, showing large scale vortices at the interface between the marina and the adjacent channel.

For Layout 4, the computed value of k was not wholly consistent with the trend observed for the other layouts (Fig. 8). This may be explained by the entrance being more centred on the marina, resulting in two counter-rotating circulation cells within the basin (Fig. 9). Reduced rates of exchange for marinas with central entrances compared to

offset entrances have been identified for marinas subject to tide-driven exchange [5, 20, 28, 29]. For such cases, it has been proposed by others to treat the marina as two mirror-image basins with offset entrances [5]. If we apply this approach for Layout 4 (Fig. 10), significant correlation between k and R_{DM} is obtained ($R^2 = 0.9602$, $n = 4$, $\alpha = 0.05$).
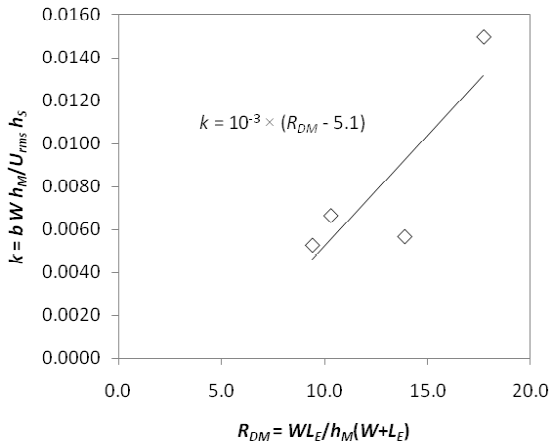

Figure 8. Dimensionless exchange coefficient k as a function of the modified shape parameter R_{DM}.

Interestingly, very few of the published guidelines and relationships for tidal exchange in marinas hold true for this study. For example, water exchange generally tended to decrease with increasing A/a, the ratio of the basin area to the entrance cross-sectional area, which conflicts with guidelines in [5] for marinas dominated by tide-driven exchange. There are significant differences in the computed mean residence times for the various layouts, despite only small changes in the tidal prism ratio.

V. CONCLUSION

A TELEMAC-2D numerical hydrodynamic model was used to evaluate flushing and mean residence times in a marina on the edge of a micro-tidal channel. The results show that, for conditions where shear-driven exchange dominates, dead zone models for water exchange provide a better means to guide optimization of marina and entrance geometry than traditional guidelines developed for tide-driven exchange.

As the time scales for flushing and water renewal at micro-tidal sites typically exceed the tidal period, the quasi-steady assumption made here is not strictly valid, and further research is needed to extend the dead zone model to oscillatory flow in a rigorous way. Other opportunities to improve the model are to consider the effects of partially developed mixing layers and flow interactions with the downstream edges of marina entrances on dead zone residence times.

Further work could be undertaken to generalise the dead zone exchange model to different entrance configurations (*e.g.* offset entrances, centred entrances and multiple entrances) and to irregularly shaped marinas (*i.e.* where W

and L cannot be clearly defined), and to investigate the transition from tide- to shear-driven flushing regimes.
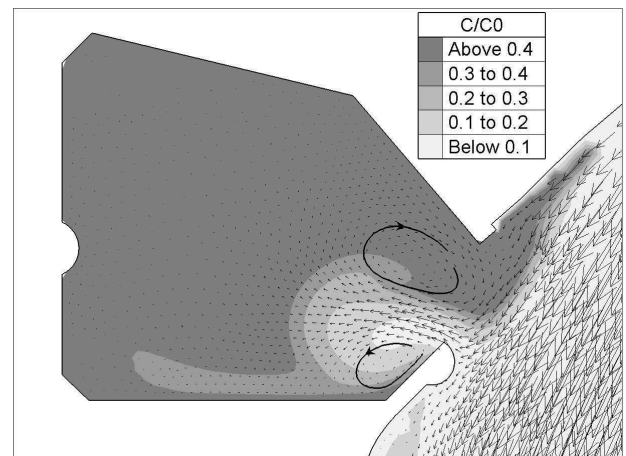

Figure 9. Snapshot of relative tracer concentrations and current vectors for Layout 4, showing counter-rotating circulation cells.
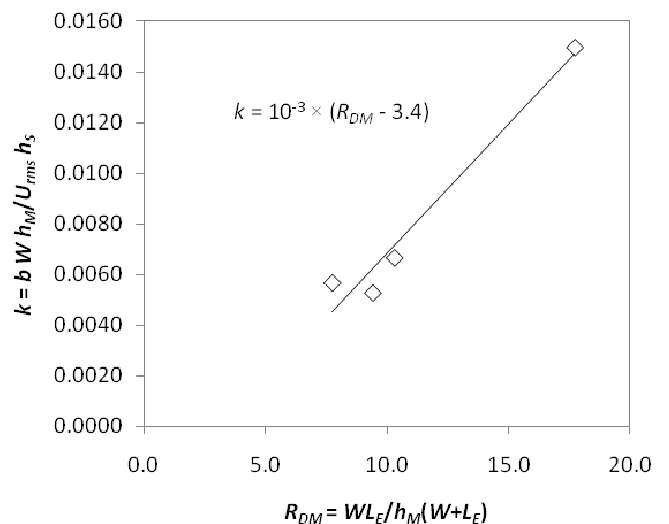

Figure 10. Dimensionless exchange coefficient k as a function of the modified shape parameter R_{DM}, with adjustment to the value for Layout 4 for a centred marina entrance.

REFERENCES

[1] T. C. Atkinson, and P. M. Davis, "Longitudinal dispersion in natural channels: 1. Experimental results from the River Severn, U.K.," Hydrol. and Earth Sys. Sci., vol. 4, pp. 345–353, 2000.

[2] R. W. Barber, and M. J. Wearing, "A mathematical model for predicting the pollution exchange coefficient of small tidal embayments," Proc. Int. Conf. Protection and Restoration of the Environment VI, pp. 355–362, Skiathos, July 2002.

[3] Canadian Hydraulics Centre, National Research Council, Blue Kenue™ Reference Manual, August 2010.

[4] S. C. Chikwendu, and G. U. Ojiakor, "Slow-zone model for longitudinal dispersion in two-dimensional shear flows," J. Fluid Mech., vol. 152, pp. 15–38, 1985.

[5] J. C. Cox, H. N. Smith, A. F. Nielsen, M. A. Pirrello, S. Desloovere, C. Mead, and A. van Tonder, "Protecting water quality in marinas," Report of International Working Group 98 convened by the Recreational Navigation Commission, Permanent International Association of Navigational Congresses, 2008.

[6] P. M. Davis, T. C. Atkinson, and T. M. L. Wigley, "Longitudinal dispersion in natural channels: 2. The roles of shear flow dispersion and dead zones in the River Severn, U.K.," Hydrol. and Earth Sys. Sci., vol. 4, pp. 355–371, 2000.

[7] P. M. Davis, and T. C. Atkinson, "Longitudinal dispersion in natural channels: 3. An aggregated dead zone model applied to the River Severn, U.K.," Hydrol. and Earth Sys. Sci., vol. 4, pp. 373–381, 2000.

[8] E.D.F.–D.R.D., TELEMAC-2D Software Version 5.2 User Manual.

[9] H. B. Fischer, E. J. List, R. C. Y. Koh, J. Imberger, and N. H. Brooks, Mixing in Inland and Coastal Waters, Academic Press, 1979.

[10] M. Ghisalberti, and H. M. Nepf, "Mixing layers and coherent structures in vegetated aquatic flows," J. Geophys. Res., vol. 107, no. C2, pp. 1–11, 2002.

[11] M. Ghisalberti and H. M. Nepf, "The limited growth of vegetated shear layers," Water Resour. Res., vol. 40, pp. 1–12, 2004.

[12] M. Ghisalberti and H. Nepf, "Mass transport in vegetated shear flows," Env. Fluid Mech., vol. 5, pp. 527–551, 2005.

[13] J. W. Harvey, B. J. Wagner, and K. E. Bencala, "Evaluating the reliability of the stream tracer approach to characterize stream-subsurface water exchange," Water Resour. Res., vol. 32, pp. 2441–2451, 1996.

[14] J. W. Harvey, J. E. Saiers, and J. T. Newlin, "Solute transport and storage mechanisms in wetlands of the Everglades, south Florida," Water Resour. Res., vol. 41, W05009, pp. 1–14, 2005.

[15] J. M. Hervouet, Hydrodynamics of Free Surface Flows: Modelling with the Finite Element Method, John Wiley & Sons, 2007.

[16] P. K. Kundu, and I. M. Cohen, Fluid Mechanics, 3rd ed., Elsevier Academic Press, 2004.

[17] R. J. Lowe, J. R. Koseff, and S. G. Monismith, "Oscillatory flow through submerged canopies: 2. Canopy mass transfer," J. Geophys. Res., vol. 110, C10017, pp. 1–14, 2005.

[18] S. C. Morris, "Shear-layer instabilities: particle image velocimetry measurements and implications for acoustics," Annu. Rev. Fluid Mech., vol. 43, pp. 529–550, 2011.

[19] E. Murphy, M. Ghisalberti, and H. Nepf, "Model and laboratory study of dispersion in flows with submerged vegetation," Water Resour. Res., vol. 43, pp. 1–12, 2007.

[20] R. E. Nece, H. N. Smith, and E. P. Richey, "Tidal circulation and flushing in five western Washington marinas," University of Washington Water Resources Series Technical Report No. 63, Seattle, June 1980.

[21] H. Nepf, M. Ghisalberti, B. White, and E. Murphy, "Retention time and dispersion associated with submerged aquatic canopies," Water Resour. Res., vol. 43, pp. 1–10, 2007.

[22] A. F. Nielsen, and A. D. McCowan, "A natural flushing system for artificial harbours: a case study of the Anchorage Port Stephens, Corlette, N.S.W.", Trans. Multi-Disc. Eng., Australia, vol GE18, pp. 41–48, 1994.

[23] J. H. Pollard, A Handbook of Numerical and Statistical Techniques with Examples Mainly from the Life Sciences, Cambridge University Press, 1977.

[24] A. Purnama, "The effect of dead zones on longitudinal dispersion in streams," J. Fluid Mech., vol. 186, pp. 351–377, 1988.

[25] M. R. Raupach, J. J. Finnigan, and Y. Brunet, "Coherent eddies and turbulence in vegetation canopies: The mixing layer analogy," Boun. Layer Meteor., vol. 78, pp. 351–382, 1996.

[26] B. H. Schmid, "Persistence of skewness in longitudinal dispersion data: can the dead zone model explain it after all?" J. Hydraul. Eng., vol. 128, pp. 848–854, 2002.

[27] I. W. Seo, and T. S. Cheong, "Moment-based calculation of parameters for the storage zone model for river dispersion," J. Hydraul. Eng., vol. 127, no. 6, pp. 453–465, 2001.

[28] U.S.E.P.A., Coastal Marinas Assessment Handbook, EPA 904/6-85-132, 1985.

[29] U.S.E.P.A., National Management Measures Guidance to Control Nonpoint Source Pollution from Marinas and Recreational Boating, EPA 841-B-01-005, November 2001.

[30] E. M. Valentine, and I. R. Wood, "Longitudinal dispersion with dead zones," J. Hydraul. Div., vol. 103, pp. 975–989, September 1977.

[31] A. van Mazijk, and E. J. M. Veling, "Tracer experiments in the Rhine Basin: evaluation of the skewness of observed concentration distributions," J. Hydrol., vol. 307, pp. 60–78, September 2004.

[32] V. Weitbrecht, S. A. Socolofsky, and G. H. Jirka, "Experiments on mass exchange between groin fields and main stream in rivers," J. Hydraul. Eng., vol. 134, pp. 173–183, 2008.

[33] V. Weitbrecht, W. Uijttewaal, and G. H. Jirka, "A random walk approach for investigating near- and far-field transport phenomena in rivers with groin fields," Proc. River Flow 2004 IAHR Conference, Naples, pp. 1–10, 2004.

[34] V. Weitbrecht, W. Uijttewaal, and G. H. Jirka, "2-D particle tracking to determine transport characteristics in rivers with dead zones," In International Symposium on Shallow Flows, Delft, 2003.

[35] A. Worman, " Comparison of models for transient storage of solutes in small streams," Water Resour. Res., vol. 36, pp. 455–468, 2000.